The Astrophysical Journal, 790:164 (7pp), 2014 August 1 doi:10.1088/0004-637X/790/2/164

FIRST DETECTION OF THE WHITE DWARF COOLING SEQUENCE OF THE GALACTIC BULGE*

A. Calamida[1], K. C. Sahu[1], J. Anderson[1], S. Casertano[1], S. Cassisi[2], M. Salaris[3], T. Brown[1], J. Sokol[1], H. E. Bond[1,4], I. Ferraro[5], H. Ferguson[1], M. Livio[1], J. Valenti[1], R. Buonanno[2], W. Clarkson[6], and A. Pietrinferni[2]
[1] Space Telescope Science Institute, 3700 San Martin Drive, Baltimore, MD 21218, USA; calamida@stsci.edu
[2] Osservatorio Astronomico di Teramo—INAF, Via M. Maggini, I-64100 Teramo, Italy
[3] Astrophysics Research Institute, Liverpool John Moores University, 146 Brownlow Hill, Liverpool L3 5RF, UK
[4] Department of Astronomy and Astrophysics, Pennsylvania State University, University Park, PA 16802, USA
[5] Osservatorio Astronomico di Roma—INAF, Via Frascati 33, I-00040 Monte Porzio Catone, Italy
[6] University of Michigan-Dearborn, 4901 Evergreen Road, Dearborn, MI 48128, USA
Received 2014 May 9; accepted 2014 June 24; published 2014 July 17

ABSTRACT

We present *Hubble Space Telescope* data of the low-reddening Sagittarius window in the Galactic bulge. The Sagittarius Window Eclipsing Extrasolar Planet Search field ($\sim 3' \times 3'$), together with three more Advanced Camera for Surveys and eight Wide-Field Camera 3 fields, were observed in the $F606W$ and $F814W$ filters, approximately every two weeks for 2 yr, with the principal aim of detecting a hidden population of isolated black holes and neutron stars through astrometric microlensing. Proper motions were measured with an accuracy of $\approx$0.1 mas yr^{-1} ($\approx$4 km s^{-1}) at $F606W \approx 25.5$ mag, and better than $\approx$0.5 mas yr^{-1} ($\approx$20 km s^{-1}) at $F606W \approx 28$ mag, in both axes. Proper-motion measurements allowed us to separate disk and bulge stars and obtain a clean bulge color–magnitude diagram. We then identified for the first time a white dwarf (WD) cooling sequence in the Galactic bulge, together with a dozen candidate extreme horizontal branch stars. The comparison between theory and observations shows that a substantial fraction of the WDs ($\approx$30%) are systematically redder than the cooling tracks for CO-core H-rich and He-rich envelope WDs. This evidence would suggest the presence of a significant number of low-mass WDs and WD–main-sequence binaries in the bulge. This hypothesis is further supported by the finding of two dwarf novae in outburst, two short-period ($P \lesssim 1$ day) ellipsoidal variables, and a few candidate cataclysmic variables in the same field.

Key words: stars: abundances – stars: evolution

Online-only material: color figures

1. INTRODUCTION

Most stars end their lives as white dwarfs (WDs). The characterization of WD populations is a valuable tool for understanding the formation history of different components of our Galaxy. Our knowledge is most extensive for the WD population of the Galactic disk, in which numerous WDs have been discovered through imaging surveys and characterized through spectroscopy (Eisenstein et al. 2006; Kepler et al. 2007; Koester et al. 2009). An updated catalog from the Sloan Digital Sky Survey Data Release 7, including 12,843 DA (H-rich envelope) and 923 DB (He-rich envelope) WDs, has been presented recently by Kleinman et al. (2013). They find a mean mass of $\sim 0.6 M_{\odot}$ for DA and $\sim 0.68\ M_{\odot}$ for DB WDs, consistent with CO cores. There is also a secondary peak in the Galactic-disk WD mass distribution around $0.4\ M_{\odot}$ (Kepler et al. 2007; Rebassa-Mansergas et al. 2011). These low-mass WDs likely have helium cores and, given that in standard stellar evolution they cannot be formed from single stars in less than a Hubble time, they have been considered to result from close-binary interactions after a common-envelope (CE) phase (post common-envelope binaries, PCEBs), or of a merger of two very low-mass He-core WDs following a second CE ejection (Han 2008). The binary scenario is supported by the finding of numerous low-mass WDs in binary systems in the field, with the companion being another WD, a neutron star, or a subdwarf B star (Marsh et al. 1995; Maxted et al. 2002). However, single He-core WDs have also been observed (Marsh et al. 1995; Kilic et al. 2007), raising the possibility that severe mass loss on the first ascent of the giant branch can prevent ignition of helium burning. Extremely low-mass He-core WDs ($M \simeq 0.2\, M_{\odot}$) have only been found in binary systems (Kilic et al. 2012).

In Galactic globular clusters (GGCs) a substantial population of He-core WDs has been observed in ω Cen (Monelli et al. 2005; Calamida et al. 2008; Bellini et al. 2013), NGC 6752 (Ferraro et al. 2003), and NGC 6397 (Strickler et al. 2009), as well as in the old metal-rich open cluster NGC 6791 (Kalirai et al. 2007; Bedin et al. 2008). He-core WDs in clusters show systematically redder colors than CO-core WDs.

In the Galactic bulge, the bulk of the population is as old as GGCs but as metal-rich as the Galactic disk (Zoccali et al. 2003; Clarkson et al. 2008, hereafter CL08), with a stellar space density closer to that in the disk than in GGCs. If age plays a major role in the formation of He-core WDs, we would expect an enhanced frequency of such objects in the Galactic-bulge population. If stellar density and/or metallicity are the determinants instead, the bulge population of He-core WDs, as well as their binary fraction, should be consistent with those in the Galactic disk.

In this paper, we present the first observational detection of the WD cooling sequence in the Galactic bulge, and discuss the implications for the origin of low-mass WDs. We have also discovered several cataclysmic variable (CV) candidates including two dwarf novae, as well as two short-period ellipsoidal binary systems.

* Based on observations made with the NASA/ESA *Hubble Space Telescope*, obtained by the Space Telescope Science Institute. STScI is operated by the Association of Universities for Research in Astronomy, Inc., under NASA contract NAS 5-26555.

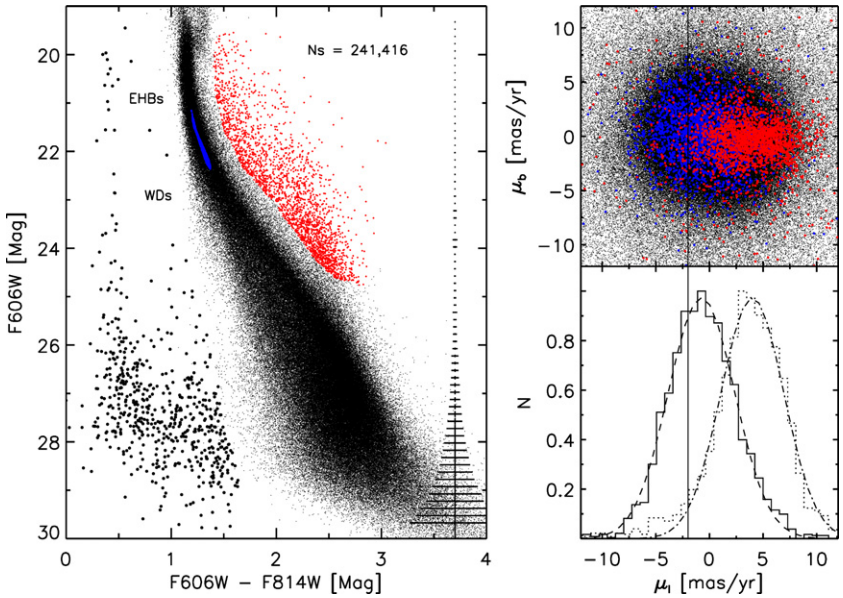

Figure 1. Left: $F606W$, $F606W - F814W$ CMD of stars selected to have high-quality photometry in the SWEEPS field. Candidate EHB and WD stars are marked with larger dots. The color cutoff was chosen not to exclude candidate WD–MS binaries. Samples of candidate bulge and disk stars are marked with blue and red dots, respectively. Right—top: PM diagram of the selected stars, with samples of candidate bulge and disk stars marked. Bottom: normalized PM histograms of Galactic longitude components for candidate bulge (left) and disk (right) stars. The two Gaussians fitting the distributions are overplotted.

(A color version of this figure is available in the online journal.)

2. OBSERVATIONS AND PHOTOMETRY

We observed the Sagittarius Window Eclipsing Extrasolar Planet Search (SWEEPS) field ($l = 0^\circ, b = -2\overset{\circ}{.}65$) in the Galactic bulge in 2004 and again in 2011, 2012, and 2013 with the *Hubble Space Telescope* (*HST*), using the Wide-Field Channel of the Advanced Camera for Survey (ACS; proposals GO-9750, GO-12586, PI: Sahu). The SWEEPS field covers $\approx 3\overset{'}{.}3 \times 3\overset{'}{.}3$ in a region of relatively low extinction in the bulge ($E(B-V) \lesssim 0.6$ mag; Oosterhoff & Ponsen 1968). The 2004 observations were taken in the $F606W$ (wide V) and $F814W$ (wide I) filters over the course of one week (for more details, see Sahu et al. 2006). The new data were collected between 2011 October and 2013 October, with a $\sim$2 week cadence, for a total of 60 $F606W$- and 61 $F814W$-band images. The 2011–2012–2013 (hereafter 2011–13) data set was reduced using a software program that performs simultaneous point-spread function (PSF) photometry on all the images (J. Anderson et al., in preparation). We adopted the 2004 photometric zero points to calibrate the data to the Vegamag system, producing a catalog of $\approx$340,000 stars down to $F606W \approx 31$ mag and the deepest color–magnitude diagram (CMD) so far published in the direction of the Galactic bulge.

A dozen images of the SWEEPS field were also collected in the $F625W$ and $F658N$ filters with the ACS camera during 2011 March (proposal GO-12020, PI: Clarkson). The reduction of this data set was performed by following the same procedure described above. The final catalog was calibrated to the Vegamag system and includes $\approx$200,000 stars down to $F625W \approx 27$ mag.

Our reduction software provides quality parameters such as the dispersion of the individual photometric and astrometric observations, the similarity of the object to the shape of the PSF and the degree of contamination of the object by neighboring stars; we use these quality parameters to cull the photometry to keep only well-measured objects. The left panel of Figure 1 shows the $F606W$, $F606W - F814W$ CMD for all the stars with high-quality photometry. The CMD shows a few interesting features: (1) there is a group of stars systematically redder than the bulge main sequence (MS) that belong to the (closer) disk population; (2) there are about a dozen candidate extreme horizontal branch (EHB) stars clearly visible in the CMD at $20 \lesssim F606W \lesssim 22$ mag and $F606W - F814W \approx 0.3$ mag; (3) there is also an indication of a WD cooling sequence starting at $F606W \approx 22.5$ mag and extending below, in the color range $0 \lesssim F606W - F814W \lesssim 1.5$ mag.

EHB stars have been identified in Baade's window of the Galactic bulge by Zoccali et al. (2003), and spectroscopically characterized as hot subdwarf stars by Busso et al. (2005). A WD population has never been identified, so it is important to determine whether they are indeed WDs and whether they belong to the bulge.

2.1. A Clean White Dwarf Bulge Sample

Stars could be in the WD region of the CMD because they are bona fide bulge or disk WDs, or because they are closer and less reddened disk MS stars. It is important then to consider a bulge sample devoid of disk stars, since some disk stars with much less reddening may appear bluer, and hence masquerade as WDs. To obtain a clean bulge sample, we estimated the proper motions (PMs) of the stars using the 2004 and 2011–13 data sets. By comparing the positions of stars in the two epochs we estimated the PMs for $\approx$200,000 stars down to $F606W \approx 28$ mag, with an accuracy $\lesssim$0.5 mas yr^{-1} ($\lesssim$20 km s^{-1}) in both axes. PMs are then projected along the Galactic coordinates shown in Figure 1 (top right panel).

We then used the CMD to select two samples of candidate stellar populations belonging to the bulge (blue dots) and the disk (red), following a procedure similar to that adopted by CL08. The two samples were selected in different magnitude and color ranges to keep the sample sizes similar, and keep the contamination of the bulge sample by disk stars minimal. The PM histograms of the Galactic-longitude components for

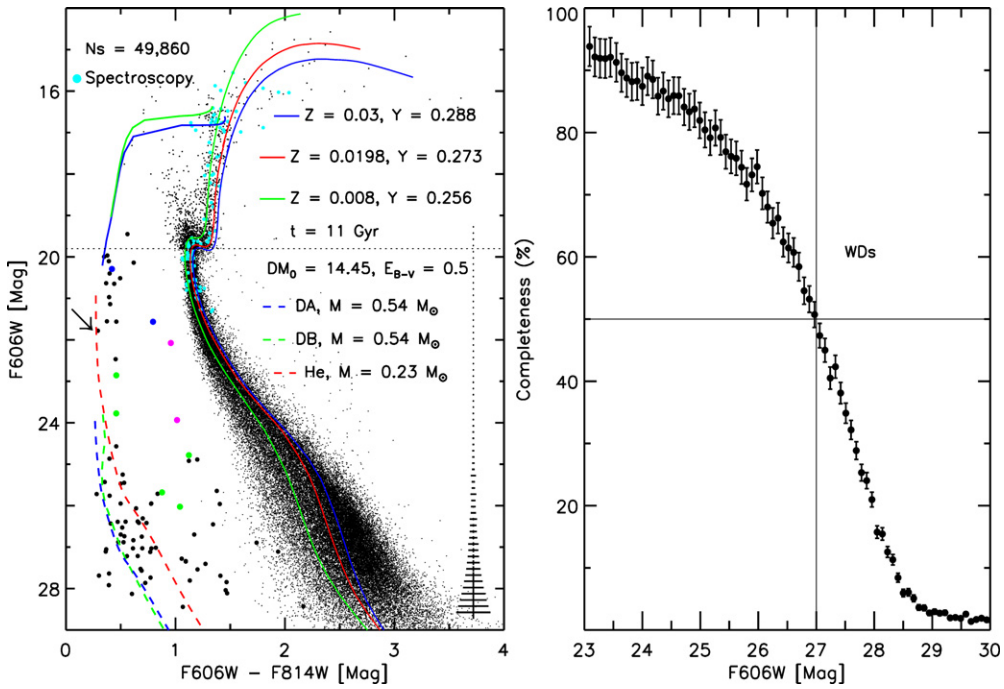

Figure 2. Left: PM-cleaned bulge CMD. Solid lines display cluster isochrones for the same age but different chemical composition. ZAHBs and cooling sequences for CO- and He-core WDs are plotted. Cyan dots mark stars with spectroscopic observations. The arrow marks the reddening vector direction. Ellipsoidal variables and dwarf novae are marked with blue and magenta dots, respectively. Green dots mark CV candidates. Right: completeness of bulge WDs. Note that 70% of the bulge WDs were rejected because of the PM selection, although most of the WDs in the selected magnitude and color range belong to the bulge. Error bars are also labeled.
(A color version of this figure is available in the online journal.)

these two populations are shown in Figure 1 (bottom right). The two populations are clearly separated, with the bulge peaking at $\mu_l \approx 0$ mas yr^{-1}, and the disk peaking at $\mu_l \approx 4$ mas yr^{-1}. The PM distribution of disk and bulge stars is a consequence of Galactic rotation, a detailed discussion of which is given in CL08. We adopted a cut at $\mu_l \leqslant -2$ mas yr^{-1} to select a nearly pure bulge sample: this selection allows us to keep ≈30% of bulge members while the residual contamination of the sample by disk stars is $\lesssim$1%. Figure 2 shows the CMD of the resulting pure-bulge sample where the photometry of stars brighter than $F606W = 19.8$ mag (which is the saturation limit for the 2011–13 data set) is taken from the 2004 data set, while the photometry of the fainter stars is from 2011–13. About 70% of the bulge WDs were indeed rejected because of the PM selection, although most of the WDs in the selected magnitude and color range belong to the bulge. To further select candidate WDs, we individually checked each star with ROMAFOT (Buonanno & Iannicola 1989) on the $F606W$ and the $F814W$ median images. Some of the candidate bulge WDs turned out to be too close to or to lie on the spikes of saturated stars, and a few others were too faint to be reliably measured ($F606W > 28$ mag); these were rejected from the sample. We note that the PM selection has led to a reduction of the number of brighter ($22 < F606W < 24$ mag) WDs from eight to four objects, two of which happen to be CVs. Table 1 lists coordinates, magnitudes, and PMs for the 72 well-measured bulge WDs. Only these well-measured WDs are included in Figure 2, which clearly shows a sequence of objects ranging from $22.5 \lesssim F606W \lesssim 29$ mag, with most of them having a color $F606W - F814W \lesssim 1.0$ mag. The only known class of objects that can occupy this part of the CMD are bulge WDs and unreddened disk stars. Since almost all ($\gtrsim$99%) disk stars were removed by the PM selection (see Section 2.1) the only remaining possibility is bulge WDs. Furthermore, faint blue galaxies, which play the role of serious contaminants in the WD sequence observed in GGCs (Richer et al. 2008), are absent in our sample since the large reddening by the Galactic disk in this direction serves as a natural filter to remove any background galaxies.

Theoretically, we expect to observe a WD cooling sequence in the bulge, since the bulge is old and formed over a relative short timescale, as suggested by the scarcity of younger stars (CL08). It is then natural to ask: why was this bulge WD sequence not identified until now? The reason is simple. It was essential to separate the disk stars in order to identify them as bulge WDs. Since the WDs are intrinsically faint, the PMs of this sample was not known. Our deep *HST* observations taken at two epochs were essential to separate the faint disk stars from the bulge WDs.

3. DISCUSSION

3.1. Theoretical Models

In order to characterize the bulge stellar population, we compared the PM-cleaned bulge CMD with evolutionary predictions. We used the BaSTI[7] (Pietrinferni et al. 2004, 2006) stellar-evolution database to fit isochrones to the CMD. Evolutionary predictions were transformed to the observational plane by adopting the color–$T_{\rm eff}$ relations provided by Hauschildt et al. (1999) for $T_{\rm eff} \leqslant 10{,}000$ K, while at larger $T_{\rm eff}$ we adopted the relations published by Bedin et al. (2005). A distance modulus of $\rm DM_0 = 14.45$ mag and a mean reddening of $E(B-V) = 0.5$ were adopted (Sahu et al. 2006). Extinction coefficients were estimated by applying the Cardelli et al. (1989) reddening relations and by adopting a standard reddening law, $R_V = A_V/E(B-V) = 3.1$, finding $A_{F606W} = 0.922\,A_V$, $A_{F814W} = 0.55\,A_V$, and $E(F606W - F814W) = 1.14\,E(B-V)$.

[7] http://albione.oa-teramo.inaf.it/

Table 1
List of the Candidate Bulge WDs in the SWEEPS Field

ID	R.A. (J2000) (hours)	Decl. (J2000) (degrees)	*F814W* (mag)	*F606W* (mag)	μ_b (mas yr^{-1})	μ_l (mas yr^{-1})
1	17:59:05.17	−29:11:36.99	19.87	20.29	0.38	−0.87
2	17:59:08.06	−29:12:55.37	20.77	21.56	−0.47	−7.23
3	17:59:02.45	−29:10:25.04	21.12	22.08	1.59	−3.77
4	17:58:53.83	−29:12:54.36	22.01	22.47	−6.22	−8.36
5	17:59:00.32	−29:10:21.97	22.40	22.86	1.50	−1.99
6	17:59:00.78	−29:12:06.03	23.32	23.77	−0.28	−4.08
7	17:59:04.63	−29:13:24.04	22.92	23.94	0.13	10.76
8	17:59:08.20	−29:13:22.86	24.11	24.57	−3.73	−3.58
9	17:58:59.20	−29:10:41.72	23.66	24.78	9.63	−3.73
10	17:59:04.60	−29:12:38.74	24.47	24.87	−1.23	−4.08
11	17:59:04.03	−29:12:33.48	23.69	24.89	−13.75	−4.12
12	17:59:06.01	−29:12:32.05	23.80	24.92	−3.91	−5.01
13	17:58:57.59	−29:10:57.57	24.73	25.25	1.80	−2.06
14	17:58:55.29	−29:13:10.85	25.08	25.43	−4.66	−5.66
15	17:59:07.84	−29:12:16.17	24.92	25.45	−2.65	−11.88
16	17:59:07.07	−29:10:53.59	24.97	25.47	1.82	−7.61
17	17:58:57.78	−29:11:39.62	24.27	25.64	2.65	−5.47
18	17:59:02.28	−29:13:07.92	24.80	25.68	−4.55	−1.82
19	17:58:52.92	−29:12:26.80	24.88	25.71	8.43	−4.16
20	17:58:54.20	−29:13:34.12	25.44	25.72	2.19	−6.32
21	17:59:02.49	−29:10:49.92	25.36	25.76	0.21	−2.29
22	17:59:00.85	−29:11:44.96	25.17	25.95	−12.02	−8.41
23	17:58:54.63	−29:11:24.61	25.45	25.95	−4.26	−5.73
24	17:59:08.40	−29:13:18.98	25.18	25.95	1.05	−5.06
25	17:58:53.57	−29:13:06.94	24.56	25.96	5.94	−3.36
26	17:58:54.29	−29:12:50.79	24.99	26.03	−11.69	−9.89
27	17:59:01.60	−29:10:46.39	25.43	26.07	2.27	−6.37
28	17:58:53.56	−29:12:53.86	25.61	26.31	−3.07	−3.66
29	17:58:53.26	−29:10:52.54	25.73	26.38	7.25	−6.56
30	17:58:55.67	−29:12:50.59	25.84	26.39	6.27	−3.49
31	17:58:59.76	−29:11:05.39	25.92	26.39	−2.59	−6.49
32	17:59:06.71	−29:11:42.42	25.75	26.42	3.48	−3.50
33	17:58:53.91	−29:12:25.18	25.68	26.42	2.14	−5.89
34	17:58:58.30	−29:11:52.83	26.02	26.43	−14.74	−3.89
35	17:59:06.25	−29:12:36.52	25.11	26.45	5.09	−3.89
36	17:59:07.12	−29:11:27.74	26.01	26.53	−3.21	−3.44
37	17:59:02.64	−29:10:20.74	26.20	26.70	0.24	−3.64
38	17:59:07.28	−29:13:29.41	25.53	26.70	−0.61	−2.23
39	17:59:06.53	−29:10:27.17	26.20	26.74	−0.74	−3.51
40	17:59:01.81	−29:13:37.94	26.06	26.75	0.64	−3.36
41	17:59:04.88	−29:10:48.33	26.22	26.83	−2.61	−7.93
42	17:59:00.05	−29:13:10.81	26.40	26.88	19.09	−2.64
43	17:58:58.19	−29:11:59.19	26.36	26.88	1.07	−1.91
44	17:58:58.16	−29:10:34.39	25.15	26.89	2.57	−5.25
45	17:59:04.61	−29:12:39.66	26.20	27.02	−3.90	−4.64
46	17:58:53.86	−29:12:09.21	26.33	27.03	0.64	−7.60
47	17:58:57.89	−29:11:20.86	26.42	27.03	−5.78	−6.14
48	17:58:56.15	−29:12:23.60	26.25	27.03	−8.36	−14.36
49	17:58:54.49	−29:12:38.40	26.69	27.05	3.14	−3.21
50	17:59:06.80	−29:12:22.94	26.74	27.11	−0.38	−4.06
51	17:58:54.57	−29:12:47.71	25.17	27.11	−1.44	−3.62
52	17:59:07.82	−29:10:27.05	26.35	27.12	3.09	−3.35
53	17:58:54.84	−29:10:55.59	26.56	27.22	−3.63	−1.81
54	17:59:07.81	−29:10:27.56	26.66	27.22	−7.48	−6.65
55	17:58:53.13	−29:11:26.66	26.22	27.28	−1.06	−2.48
56	17:59:05.43	−29:10:56.20	26.24	27.34	0.12	−7.27
57	17:59:02.03	−29:11:20.24	26.25	27.35	−3.49	−1.93
58	17:58:52.81	−29:13:29.94	26.13	27.40	7.06	−8.83
59	17:59:06.08	−29:13:11.52	26.85	27.53	−7.65	−4.96
60	17:58:58.86	−29:11:53.78	26.34	27.54	−3.36	−1.93
61	17:58:58.90	−29:10:34.16	26.88	27.57	4.64	−6.79
62	17:58:54.57	−29:11:05.00	27.24	27.64	5.03	−2.70
63	17:58:55.31	−29:12:59.55	27.39	27.69	2.03	−2.36
64	17:58:57.27	−29:12:55.87	26.28	27.69	−11.23	−8.56
65	17:59:05.34	−29:10:56.44	26.96	27.74	0.49	−3.85
66	17:59:04.02	−29:11:09.83	26.68	27.81	−3.77	−5.70
67	17:59:06.26	−29:10:17.15	26.38	27.84	−12.46	−10.81
68	17:59:03.23	−29:11:45.79	27.14	27.86	−0.18	−2.31
69	17:59:06.04	−29:10:55.55	27.53	27.92	−5.54	−7.13
70	17:59:01.57	−29:10:44.23	26.58	28.04	3.82	−8.56
71	17:59:05.66	−29:12:10.14	26.64	28.11	0.88	−3.19
72	17:59:01.93	−29:10:50.29	27.53	28.13	6.01	−3.06
73	17:58:57.95	−29:11:53.87	26.26	28.43	8.99	−9.13
74	17:59:05.52	−29:10:53.30	27.37	28.44	−0.64	−4.76

Note. The first two stars are the ellipsoidal variables.

Solid lines in Figure 2 show isochrones for an age of $t = 11$ Gyr and a scaled-solar mixture with different chemical compositions. The blue line corresponds to $Z = 0.03, Y = 0.288$ ([Fe/H] $= 0.26$), the red to $Z = 0.0198, Y = 0.273$ ([Fe/H] $= 0.06$), and the green to $Z = 0.008, Y = 0.256$ ([Fe/H] $= -0.35$). Zero-age horizontal branches (ZAHBs) are plotted for the most metal-poor (green) and the most metal-rich chemical compositions (blue). We adopted these mixtures based on the medium-resolution spectroscopy of 93 turn-off (TO), red-giant (RG) and MS stars in the SWEEPS field, collected with FLAMES/VLT (ESO, cyan dots). The distribution spans a range of $-1.0 <$ [M/H] < 0.8, and shows three main peaks at [M/H] ≈ -0.5, 0.0, and $\approx$0.25. This distribution is in fairly good agreement with the spectroscopic metallicity distributions found by Hill et al. (2011), Bensby et al. (2013), and Ness et al. (2013) for the bulge.

To fit the bulge WD cooling sequence, we adopted the BaSTI cooling tracks for DA and DB CO-core WDs and the models of Althaus et al. (2009) for He-core WDs. For $t \approx 11$ Gyr, and solar metallicity, the mass of the stars at the TO is $\approx 0.95\,M_\odot$ and the theoretical initial-to-final mass relationships predicts WD masses of $\sim$0.53–0.55$M_\odot$ (Weiss & Ferguson 2009). This prediction is observationally supported by the spectroscopic measurements of bright WDs in the GGC M4 by Kalirai et al. (2009), for which they find a mean mass of $\sim 0.53\,M_\odot$. So we used cooling tracks for DA and DB CO-core WDs with mass $M = 0.54\,M_\odot$ (Salaris et al. 2010), and He-core WD tracks for a mass of $0.23\,M_\odot$. We applied to the cooling tracks the same distance modulus and reddening adopted for the isochrones.

The comparison between theory and observation shows that old scaled-solar isochrones spanning almost 1 dex in metallicity, $-0.4 \lesssim$ [Fe/H] $\lesssim 0.3$, fit the bulge MS and red giant branch (RGB) quite well over most of the color range. However, there are stars systematically bluer or redder than the most metal-poor and metal-rich isochrones. Part of this residual color spread is due to photometric errors, differential reddening and depth effects.

Figure 2 also shows that cooling tracks for DA (dashed blue line) and DB (dashed green) CO-core WDs, which are expected to be shifted up to $\pm$0.5 mag due to the bulge depth, are unable to reproduce the entire color range of the observed WD cooling sequence. An increase in the mean mass of the WDs would move the models toward bluer colors, further increasing the discrepancy. We then assume the presence of a fraction of low-mass, $M \lesssim 0.45\,M_\odot$, WDs in the bulge. The lower mass He-core cooling track for $M = 0.23\,M_\odot$ (dashed red) fits the

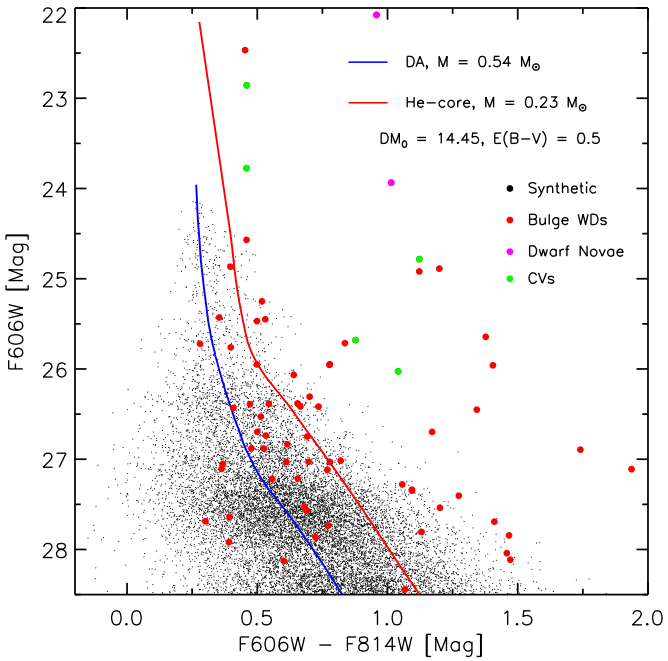

Figure 3. $F606W$, $F606W-F814W$ CMD of ~30,000 synthetic WDs. Bulge WDs are overplotted with red dots. Green and magenta dots mark candidate CVs and the dwarf novae. CO-core DA (blue line) and an He-core (red) cooling tracks are over-plotted.

(A color version of this figure is available in the online journal.)

red side of the bulge WD sequence, but it is not able to account for the reddest WDs. Note that empirical evidence shows that the lower mass limit for WDs is $\approx 0.2\,M_{\odot}$ (Kepler et al. 2007).

3.2. The Color Spread of the WD Cooling Sequence

To properly characterize the color spread and the completeness of the bulge WD cooling sequence, shown in the right panel of Figure 2, we performed several artificial star (AS) tests to estimate the magnitude and color dispersion of the sequence due to photometric errors and to the reduction and selection techniques adopted. We randomly added ≈160,000 artificial WDs to all images, with magnitudes and colors estimated by adopting a DA cooling track with $M = 0.54\,M_{\odot}$, and by adding a distance modulus of 14.45 mag and a mean reddening of $E(B-V) = 0.5$. Artificial stars are added and recovered on the images one at a time, not to affect the crowding, by using the same reduction procedures adopted earlier. We then estimated the magnitude and color spread of the artificial WD cooling sequence. This information was used as input to produce a synthetic sequence from the DA cooling track. After correcting the model absolute magnitudes for distance modulus and reddening, we have drawn randomly 30,000 ages with a uniform probability distribution, within the age range corresponding to the observed WD magnitude range. The resulting magnitudes were then perturbed with a Gaussian photometric error obtained from the AS tests.

Figure 3 shows the synthetic WD sequence, which also includes the effect of differential reddening. We added to the star magnitudes extinction values simulated as clumps with a maximum peak of $A_V \sim 0.6$ mag on top of a uniform reddening of $A_V \sim 1.5$ mag. The assumption of an extinction increase up to $A_V = 1$ mag for ≈30% of the WDs, which would explain the presence of the reddest WDs, must be discarded since we do not see any evidence for the presence of such differential reddening along the MS for a similar fraction of stars.

Candidate bulge WDs are overplotted as red dots on the synthetic cooling sequence of Figure 3, together with a DA CO-core (blue line) and a He-core (red) track. Figure 3 shows that differential reddening added to photometric errors cannot account for the entire color spread of the observed WD sequence in the bulge, by assuming only a CO-core WD population with a mean mass of $\sim 0.54\,M_{\odot}$. It is worth noting that if the spread were due only to the aforementioned factors, we would observe an equivalent number of WDs bluer than the cooling tracks.

The agreement between theory and observations improves by assuming that a fraction of the WDs have lower masses. This moves the theoretical tracks bright-ward and to the red, thus improving the agreement with our observations. These stars could be He-core WDs as described in Section 3.1, but a fraction of them could also be low-mass CO-core WDs. The recent theoretical calculations of Prada Moroni & Straniero (2009) showed indeed that CO-core WDs with masses down to $\sim 0.33\,M_{\odot}$ can form in high-density environments, when a strong episode of mass loss occurs along the RGB, due to binary interactions. However, this theoretical scenario requires very fine-tuned initial conditions, suggesting that these stars are more likely to be He-core WDs.

3.3. Binaries as Precursors of He-core WDs

It is not possible to explain the presence of He-core WDs, which are expected to have masses $\lesssim 0.45 M_{\odot}$, as a result of single-star evolution in less than a Hubble time. As described earlier, a natural explanation for the presence of such WDs is that they result from close-binary interactions after a CE phase, or from a merger of two very low-mass He-core WDs following a second CE ejection. In this scenario, a small number of the He-core WDs are expected to show signatures of variability consistent with WD–MS and CV binaries, or ellipsoidal variables.

To look for the presence of binaries in the bulge WD sample, we checked the brightest WDs ($F606W \lesssim 26$ mag) for variability, and we indeed identified two ellipsoidal variables (blue dots in Figure 2), two dwarf novae in outburst (magenta dots in Figures 2 and 3), and five candidate CVs in quiescence (green dots in Figures 2 and 3). These findings support the presence of He-core WDs in the bulge. Moreover, the luminosity of the accretion disk and the companion in the WD–MS systems moves the WDs toward redder colors in the optical CMD (Darnley et al. 2012), which would be consistent with our observations of the very red WDs.

The V and I light curves of one ellipsoidal variable based on the 2004 data set are shown in Figure 4. The estimated period and amplitude are $P = 2.258 \times 10^{-1} \pm 2 \times 10^{-5}$ days and $A = 5.1 \times 10^{-2} \pm 9 \times 10^{-4}$ mag. By assuming that the primary star is a WD and the companion a MS star, we estimated a semi-major axis $a = 0.007$ AU, and masses of ≈ 0.3–$0.4\,M_{\odot}$ and ≈ 0.6–$0.7\,M_{\odot}$ for the two components, respectively. An accurate estimate of the masses of the components of these systems needs radial velocities; we are in the process of collecting such data through spectroscopic observations with GMOS at GEMINI South. It is noteworthy that the $V-I$ color of the variable is constant (see Figure 4), which means that we cannot be observing a reflection effect, i.e., the heated hemisphere of the MS companion as in the case of the WD–MS binary HS 1857+5144 (Aungwerojwit et al. 2007). This ellipsoidal variable is relatively bright with $F606W \sim 21.6$ mag; stars belonging to the reddest WD cooling sequence could be the fainter counterparts of this object. Unfortunately, we do not have

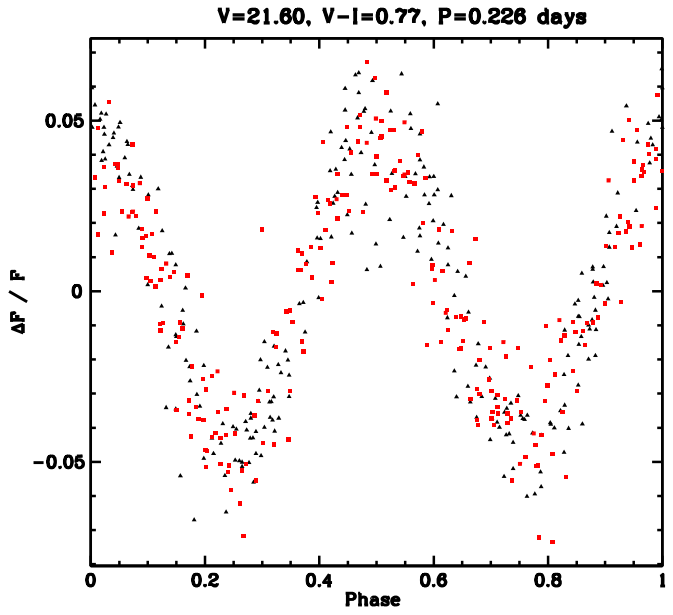

Figure 4. $F606W$ (V, red rectangles) and $F814W$ (I, black triangles) phased light curves of one of the ellipsoidal variables identified in the SWEEPS field. This variable is located between the bulge EHB–WD sequences and the MS (see Figure 1).

(A color version of this figure is available in the online journal.)

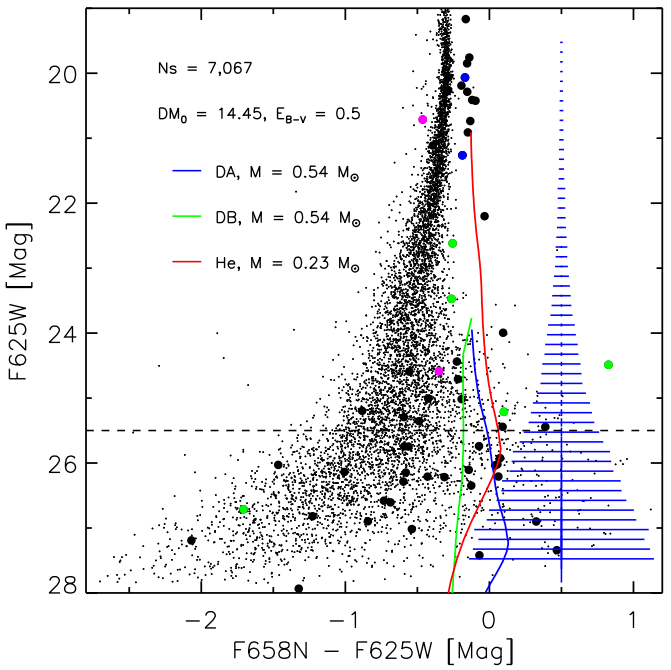

Figure 5. $F625W$, $F658N - F625W$ CMD for the SWEEPS field. Bulge WDs and EHBs are the larger black dots. Green and magenta dots mark candidate CVs and the dwarf novae, while the blue dots mark the two ellipsoidal variables. CO-core DA (blue line), DB (green) and He-core (red) cooling tracks are overplotted. Error bars are also labeled.

(A color version of this figure is available in the online journal.)

2004 time-series photometry for the fainter candidate CVs to verify this hypothesis. The 2011–13 data set has a two-week observation cadence, so we were unable to probe all possible periods for our candidate variables. candidates for short-period variability. Population-synthesis models predict that most WD–MS systems have periods in the range 2–30 hr (Yungelson et al. 1994). Moreover, models from Iben et al. (1997) predict that ≈75% of the WDs in close binaries are low-mass He-core WDs. This scenario is observationally supported by Rebassa-Mansergas et al. (2011) who measured masses for ∼200 wide WD–MS systems and PCEBs; they find that the mass distribution of the complete sample of binaries is bimodal, with a main peak at $M \sim 0.55\ M_{\odot}$ and a secondary one at $M \sim 0.40\ M_{\odot}$, while the distribution of the PCEBs shows a concentration of systems toward the low-mass end, with only few binaries with $M \gtrsim 0.55\ M_{\odot}$ (see their Figure 1).

WD–MS binaries and PCEBs might exhibit H_{α} excess (Rebassa-Mansergas et al. 2007). To check for the presence of H_{α} excess among our sample of bulge WDs, we matched the $F606W$, $F814W$-band 2011–2013 data set with the $F625W$-, $F658$-band catalog, finding ≈200,000 stars in common. Using the PMs from the 2011–2013 data set, the matched catalog was cleaned to keep only the bulge stars.

Figure 5 shows the $F625W$, $F658N - F625W$ PM-cleaned CMD for the SWEEPS field. The $F625W$, $F658N - F625W$ CMD is designed to specifically highlight the presence of H_{α} bright stars. In this plane, EHBs and the WDs are expected to be toward the right/red of the MS since they have stronger H_{α} absorption line. Out of 72, 48 bulge WDs and 10 out of 12 EHBs were identified in this sample and are marked as larger filled dots in the figure. The two ellipsoidal variables (blue dots), the dwarf novae (magenta) and four out of five candidate CVs (green) were identified too. WDs fainter than $F606W \leqslant 27$ mag were not detected either in the $F625W$-band or in the $F658N$-band. The same WD cooling tracks adopted to fit the other CMDs are overplotted. The figure shows that the WD cooling tracks agree with the observations within the uncertainties in the magnitude range $22 \lesssim F625W \lesssim 27$ mag. However, there is a fraction of WDs that is systematically toward the left/blue of the CO-core and He-core cooling tracks. The photometric error is $\sigma_{F606W-F814W} \lesssim 0.2$ mag at $F625W \approx 25.5$ mag (shown by a dotted horizontal line in the figure), but some WDs are shifted toward the blue of the CMD by more than 2σ.

For magnitudes brighter than $F625W = 25.5$, there are a total of 17 WDs. Six of these WDs, including both the observed dwarf novae, show H_{α} excess, with $F658N - F625W \lesssim -0.3$ mag. This implies that ≈30% of the WDs show H_{α} excess. This result further supports the hypothesis of the presence of a fraction of PCEBs and WD–MS binaries in the bulge. For magnitudes fainter than $F625W = 25.5$, there is a trend of the WD cooling sequence toward bluer colors. This may be either due to blending with other stars, presence of stars with H_{α} excess as described above, or other yet unknown effects. It is worth noting that one of the CV candidates ($F606W \sim 24.5$ mag) shows very strong H_{α} absorption, with $F658N - F625W \approx 0.8$ mag. This object resembles the three CVs identified by (Taylor et al. 2001) in the NGC 6397, which all have $F658N - F625W > 0.5$ mag.

3.4. Number Counts

To further investigate the potential presence of a substantial fraction of He-core WDs in the bulge, we compared WD counts for $F606W \leqslant 27$ mag, corrected for completeness, to MS counts across the TO region ($19.9 < F606W < 20.15$ mag), where the evolution of the star is faster and almost independent of the initial mass function (Calamida et al. 2008).

Note that we are taking into account only 30% of bulge stars due to our PM selection, but this does not matter for a comparative analysis since the same PM selection should affect equally all evolutionary phases.

We selected the brightest PM-selected WDs ($22.5 < F606W < 27$ mag) in seven magnitude limits corresponding to $F606W < 24$, 24.5, 25, 25.5, 26, 26.5, and 27, and counted how many stars there are up to each limit. We then associated to each magnitude limit a WD cooling time, t_{WD}, from the BASTI DA CO-core cooling track for a mass of 0.54 $M_{\odot}$. It is interesting to note that the cooling time at $F606W \approx 28$ mag for this sample of WDs is ≈500 Myr, assuming most stars are 0.54 $M_{\odot}$ DA CO-core WDs, and assuming a distance modulus and reddening of $DM_0 = 14.45$ mag and $E(B-V) = 0.5$ mag, respectively.

The mean MS mass at the TO magnitude range $19.9 < F606W < 20.15$ mag is 0.95 $M_{\odot}$, according to a BASTI scaled-solar isochrone for $t = 11$ Gyr and $Z = 0.02$, and the same distance modulus and reddening as described above. We then adopted a BASTI evolutionary track for the same composition and for a mass of 0.95 $M_{\odot}$ to estimate the time that takes for MS stars to cross the magnitude range from $F606W$ =19.9 to 20.15 as $t_{MS} \sim 1 \times 10^9$ yr.

The comparison between observed star counts corrected for completeness, $N_{\rm WD}/N_{\rm MS}$, and the theoretical lifetime ratios, $t_{\rm WD}/t_{\rm MS}$, shows that we are observing about a factor two more WDs than predicted if all the WDs are CO core.

We now assume the presence of a fraction of ∼30% He-core WDs with a mass of 0.4 $M_{\odot}$ in the sample based on the discussion above, for which the cooling times are significantly longer compared to those of CO-core WDs. We then estimate the total WD cooling time as $t_{\rm tot} = 0.30 \times t_{\rm cool}$(He-core) + $0.70 \times t_{\rm cool}$(CO-core) The observed and theoretical ratios then agree within the uncertainties taking into account a 10% uncertainty in the WD cooling times and MS lifetimes, and the Poisson statistics on the number counts.

This argument thus further strengthens the hypothesis of the presence of a fraction of He-core WDs in the Galactic bulge.

4. SUMMARY

We have identified for the first time a potential WD cooling sequence in the Galactic bulge, based on *HST* $F606W$-, $F814W$-band images of the low-reddening Sagittarius window, taken at two different epochs. The WD sequence extends from $F606W \approx 22.5$ to 29 mag, with a color range of $0 \lesssim F606W - F814W \lesssim 1.5$ mag. Separating the disk and bulge stars through PMs down to very faint magnitudes was crucial in identifying the bulge WDs. We also identified a dozen candidate EHBs, two ellipsoidal variables, two dwarf novae and five candidate CVs.

The color spread of the WD sequence is rather large, and cannot be explained simply by photometric errors, differential reddening and depth effects if all the WDs are CO core. The large color spreads indicates that some of the observed WDs are be He core, which are expected to be redder.

However, there are a few very red WDs ($F606W - F814W \gtrsim 1.0$ mag), which cannot be explained even by assuming they are very low-mass (∼0.2 $M_{\odot}$) He-core WDs. Among the brighter of the very red objects we find one ellipsoidal variable, probably composed of a WD accreting from a MS companion, and two dwarf novae. The fainter counterparts of these binaries could populate the region where the reddest WDs are observed in the CMD. These systems could be WDs which are in binary systems, composed of a WD and a low-mass ($M < 0.3\,M_{\odot}$) MS companion. This hypothesis is further supported by the discovery of five candidate CVs in the field, based on the 2011–13 time-series photometry. The dwarf novae and a fraction of bulge WDs also show a mild H_{α} excess as expected.

A detailed analysis shows that the ratio of WD and MS star counts is about a factor of two larger than the ratio of CO-core WD cooling times and MS lifetimes if all the WDs are CO core. The observed number is consistent with the expected number if we assume the presence of ≈30%–40% He-core WDs in the bulge, as already suspected from the color spread of the WDs and the presence of CVs and ellipsoidal variables.

This study was supported by NASA through grants GO-9750 and GO-12586 from the Space Telescope Science Institute, which is operated by AURA, Inc., under NASA contract NAS 5-26555. We thank B. Gänsicke for useful suggestions and discussions about WD–MS binaries. We thank the anonymous referee for helpful suggestions which led to an improved version of the paper.

REFERENCES

Althaus, L. G., Panei, J. A., Romero, A. D., et al. 2009, A&A, 502, 207
Aungwerojwit, A., Gänsicke, B. T., Rodríguez-Gil, P., et al. 2007, A&A, 469, 297
Bedin, L. R., Cassisi, S., Castelli, F., et al. 2005, MNRAS, 357, 1038
Bedin, L. R., Salaris, M., Piotto, G., et al. 2008, ApJL, 679, L29
Bellini, A., Anderson, J., Salaris, M., et al. 2013, ApJL, 769, L32
Bensby, T., Yee, J. C., Feltzing, S., et al. 2013, A&A, 549, A147
Buonanno, R., & Iannicola, G. 1989, PASP, 101, 294
Busso, G., Moehler, S., Zoccali, M., Heber, U., & Yi, S. K. 2005, ApJL, 633, L29
Calamida, A., Corsi, C. E., Bono, G., et al. 2008, ApJL, 673, L29
Cardelli, J. A., Clayton, G. C., & Mathis, J. S. 1989, ApJ, 345, 245
Clarkson, W., Sahu, K., Anderson, J., et al. 2008, ApJ, 684, 1110
Darnley, M. J., Ribeiro, V. A. R. M., Bode, M. F., Hounsell, R. A., & Williams, R. P. 2012, ApJ, 746, 61
Eisenstein, D. J., Liebert, J., Harris, H. C., et al. 2006, ApJS, 167, 40
Ferraro, F. R., Possenti, A., Sabbi, E., & D'Amico, N. 2003, ApJL, 596, L211
Han, Z. 2008, A&A, 484, L31
Hauschildt, P. H., Allard, F., Ferguson, J., Baron, E., & Alexander, D. R. 1999, ApJ, 525, 871
Hill, V., Lecureur, A., Gómez, A., et al. 2011, A&A, 534, A80
Iben, I., Jr., Tutukov, A. V., & Yungelson, L. R. 1997, ApJ, 475, 291
Kalirai, J. S., Bergeron, P., Hansen, B. M. S., et al. 2007, ApJ, 671, 748
Kalirai, J. S., Saul Davis, D., Richer, H. B., et al. 2009, ApJ, 705, 408
Kepler, S. O., Kleinman, S. J., Nitta, A., et al. 2007, MNRAS, 375, 1315
Kilic, M., Brown, W. R., Allende Prieto, C., et al. 2012, ApJ, 751, 141
Kilic, M., Stanek, K. Z., & Pinsonneault, M. H. 2007, ApJ, 671, 761
Kleinman, S. J., Kepler, S. O., Koester, D., et al. 2013, ApJS, 204, 5
Koester, D., Voss, B., Napiwotzki, R., et al. 2009, A&A, 505, 441
Marsh, T. R., Dhillon, V. S., & Duck, S. R. 1995, MNRAS, 275, 828
Maxted, P. F. L., Marsh, T. R., Heber, U., et al. 2002, MNRAS, 333, 231
Monelli, M., Corsi, C. E., Castellani, V., et al. 2005, ApJL, 621, L117
Ness, M., Freeman, K., Athanassoula, E., et al. 2013, MNRAS, 430, 836
Oosterhoff, P. T., & Ponsen, J. 1968, BANS, 3, 79
Pietrinferni, A., Cassisi, S., Salaris, M., & Castelli, F. 2004, ApJ, 612, 168
Pietrinferni, A., Cassisi, S., Salaris, M., & Castelli, F. 2006, ApJ, 642, 797
Prada Moroni, P. G., & Straniero, O. 2009, A&A, 507, 1575
Rebassa-Mansergas, A., Gänsicke, B. T., Rodríguez-Gil, P., Schreiber, M. R., & Koester, D. 2007, MNRAS, 382, 1377
Rebassa-Mansergas, A., Nebot Gómez-Morán, A., Schreiber, M. R., Girven, J., & Gänsicke, B. T. 2011, MNRAS, 413, 1121
Richer, H. B., Dotter, A., Hurley, J., et al. 2008, AJ, 135, 2141
Sahu, K. C., Casertano, S., Bond, H. E., et al. 2006, Natur, 443, 534
Salaris, M., Cassisi, S., Pietrinferni, A., Kowalski, P. M., & Isern, J. 2010, ApJ, 716, 1241
Strickler, R. R., Cool, A. M., Anderson, J., et al. 2009, ApJ, 699, 40
Taylor, J. M., Grindlay, J. E., Edmonds, P. D., & Cool, A. M. 2001, ApJL, 553, L169
Weiss, A., & Ferguson, J. W. 2009, A&A, 508, 1343
Yungelson, L. R., Livio, M., Tutukov, A. V., & Saffer, R. A. 1994, ApJ, 420, 336
Zoccali, M., Renzini, A., Ortolani, S., et al. 2003, A&A, 399, 931